Hindawi
International Journal of Aerospace Engineering
Volume 2022, Article ID 7313586, 18 pages
https://doi.org/10.1155/2022/7313586

*Review Article*

# An Improved Predictor-Corrector Guidance Algorithm for Reentry Glide Vehicle Based on Intelligent Flight Range Prediction and Adaptive Crossrange Corridor

**Mingjie Li**,[1] **Chijun Zhou**,[2] **Lei Shao**,[2] **Humin Lei**,[2] **and Changxin Luo**[1]

[1]*Graduate College, Air Force Engineering University, Xi'an 710051, China*
[2]*Air and Missile Defense College, Air Force Engineering University, Shanxi, Xi'an 710051, China*

Correspondence should be addressed to Chijun Zhou; zhouchijun666@126.com

Received 4 July 2022; Revised 28 September 2022; Accepted 22 October 2022; Published 16 November 2022

Academic Editor: Xingling Shao



For traditional predictor-corrector guidance algorithm for reentry glide vehicle, it cost a lot of time to obtain predicted flight range with a slow speed to iterate. In this paper, according to residual network (ResNet)'s block and dynamic model of vehicle, through analyzing the characteristics of predicted flight range with constraints, the flight range prediction block and flight range prediction neural network are designed, which can obtain the predicted range accurately and quickly; then aiming at the separation between guidance logic and no-fly zone avoidance logic, which may lead to guidance failure and increasing of the sign variation number of the bank angle, the no-fly zone crossrange and the no-fly zone mapping crossrange are proposed in this paper. According the repulsion force of artificial potential field, an adaptive crossrange corridor combining guidance logic and no-fly zone avoidance logic is proposed, and the convergence of the corridor is analyzed theoretically. Through simulation, the block number of flight range prediction network is determined firstly. By this method, the efficiency of lateral guidance can be improved. Then, through the simulation with the different no-fly zones under different disturbed conditions, the stability and validity of the guidance method are verified. Finally, compared with other predictor-corrector algorithms, the proposed method can realize guidance with less sign variation number of bank angle and better avoidance for no-fly zones.

## 1. Introduction

The reentry glide vehicle [1] with a lift body structure has extremely fast reentry and glide speeds, and can make a jump maneuver of tens of kilometers in longitudinal direction with hundreds of kilometers maneuver range in lateral direction, which is difficult to predict and intercept [2], thus has high research value.

The research on the guidance mechanism of the reentry glide vehicle is beneficial to efficient trajectory generation and accurate guidance. At present, there are several excellent methods for guiding and controlling of agents with uncertainty. For example, Zhang et al. [3] proposed a path-following control capable of reinforcing transient performances for networked mobile robots over a single curve, in which a tracking differentiator-based prescribed performance control (TDPPC) scheme was proposed to enforce tracking deviations of geometric and dynamic objectives approximating to pregiven ranges before an appointed time. And for the control with uncertainties, a line-of-sight principle-employed realizing guidance and aperiodic sampling-based extended state observers (AS-ESOs) were developed to estimate disturbance [4], when an unknown input observer-based appointed-time funnel control policy was proposed for the control with unknown input [5]. The above trajectory guidance and control methods are suitable for discontinuous low-velocity vehicles. And in general, the guidance mode of reentry glide vehicle can be divided into nominal trajectory guidance and predictor- corrector guidance.

The nominal trajectory guidance methods usually make use of convex optimization or sequential quadratic programming method; base on the Drag-Velocity (D-V) or Height-Velocity (H-V) profile of the vehicle, find the optimal nominal

trajectory satisfying various constraints. By introducing a new state, Wang and Grant [6] performed the first-order Taylor expansion on the three-dimensional dynamic equation of the reentry vehicle, realizing convexification, and solving the approximate solution of the original problem, when its convergence is also discussed. X. Zhou et al. [7] realized optimization of the approximate solution of the vehicle within the three-dimensional profile after convexification of the three-dimensional dynamic models of the reentry vehicle, and the new variables were introduced to realize the change of the trust region. On this basis, X. Zhou et al. [8] refined the mesh point generation methods to improve the speed of trajectory generation keeping guidance accuracy. Except convex optimization, the pseudospectral method has high accuracy in solving the strongly nonlinear and strongly constrained optimal control problems and has been rapidly developed and applied in the vehicle trajectory optimization [9]. Li et al. [10] proposed a multi-interval mesh refinement radau pseudospectral method, which improved the optimization accuracy and convergence speed of the algorithm. H. Y. Zhou et al. [11] improved the particle swarm optimization algorithm to solve the trajectory planning problem in the glide phase of hypersonic vehicle. In summary, the nominal trajectory guidance method can realize guidance of reentry glide vehicle satisfying constraints. However, the optimization process of this method cost pretty a long time, and it is difficult to meet the requirement generating the trajectory fast.

To generate the guidance trajectory of reentry glide vehicle within a short time, the predictor-corrector guidance methods are usually adopted. According to different mechanisms, predictor-corrector guidance algorithms include analytical type and numerical type. The analytical predictor-corrector method sets an equation with analytical form for the guidance process and obtains approximate solution within the guidance cycle. Then, continuously corrects the equation parameters by using difference value between approximate solution and terminal constraints. Bryant et al. [12] proposed an analytic resistance equation based on the resistance height profile to realize the guidance of the reentry vehicle. Lunghi et al. [13] transformed the guidance process of reentry vehicle into an optimal control problem and obtained its semianalytical solution. Mingliang et al. [14] designed a new balanced glide adaptive guidance algorithm, which can imitate the predictor-corrector method to achieve effective guidance of reentry glide vehicle. Although the analytical predictor-corrector method has been used in the early development of reentry glide vehicle, it still has several shortcoming. The analytical process needs to be designed in advance with a unique analytical form, which leads to complicated motion equation, large analytic solution error, and sensibility for parameter disturbance.

With the enhancement of computing power, the numerical predictor-corrector algorithms are used more and more. By setting the control logic of longitudinal and lateral direction, the numerical predictor-corrector algorithms obtain the predicted range by continuously iterate the integral trajectory according to dynamic equation. Then, the control parameters are modified by calculating the difference value between range-to-go and the predicted flight range. Finally, the guidance can be realized with the lateral guidance logic.

The process of the numerical prediction correction algorithm can be divided into two stages: longitudinal guidance and lateral guidance. In the longitudinal guidance stage, the attack angle profile and the absolute value of bank angle need to be determined. In order to meet various constraints finely, the attack angle profile should be set in advance in the process of predictor-corrector guidance [15] in common. Then, all kinds of constraints are transformed into bank angle corridor [16], and the path constraints are meet by the constraints of bank angle. To calculate the absolute value of the bank angle, the common method is used to calculate the difference value of two adjacent time's predicted flight range [17] and put the difference value into the secant method. According to the secant method, Tao et al. [18] modified the absolute value of bank angle change law based on fuzzy logic to improve the accuracy of predictor-corrector method. Consider that traditional secant method is limited by initial value selection, X. Zhang et al. [19]. proposed a design formula of secant method, which is insensitive to initial value. L. Cheng et al. [20] designed a new compound bank corridor that is designed to help convert the complicated trajectory planning problem into a root-finding problem, which is identified by a recursive least squares estimation algorithm and solved by a newly proposed period-crossing steepest descent method within a fraction of a second. For the calculation of predicted range, the differential relationship between speed and range [21] and range and energy [22] is usually used. However, due to the complexity of the dynamics model, the predicted flight range cannot be obtained by analytical integration. To solve this problem, some scholars predicted the flight range by predicting the landing points position. Among them, J. Zhang et. al [23] predicted the landing point position by iteratively extrapolating at each time. Then, neural network was used to learn the functional relationship between the landing point position and initial state, which improved the speed of predictor-corrector method [24]. In the above method, the calculation time of the predicted flight range or the landing points is pretty long or the improved method has low correlation with dynamic model.

In the lateral guidance stage of reentry vehicle, heading deviation angle corridor [25] and crossrange corridor [26] are usually adopted. The guidance method based on crossrange corridor may obtain higher guidance precision, while the crossrange reflecting the lateral guidance characteristics of vehicle easily. Base on the mechanism of vehicle lateral guidance, K. Zhang et al. [27] proposed a crossrange corridor that can constrain the crossrange dynamically and improved the lateral guidance accuracy of vehicle. In the process of lateral guidance, there are usually no-fly zones that cannot be passed by vehicle, so valid no-fly zone avoidance logic needs to be set up. Among them, J. Zhu et al. [28] described the relative position relationship between the flight path of the vehicle and no-fly zones through the angle of sight and proposed the boundary selection algorithm for each no-fly zone to realize the minimum energy avoidance. For the lateral guidance instability caused by no-fly zone, H. Lin et al. [29] combined lateral guidance with heading dead zone corridor to realize no-fly zone avoidance with a small amount of bank angle sign change. The above method all designed avoidance logic for the no-fly zones when the

avoidance logic is independent to lateral guidance logic, which may cause the failure of vehicle avoidance or increasing variation number of bank angle's sign.

Aiming at long calculation time of traditional predicted flight range, through analyzing variation of predicted flight range with bank angle corridor, the flight range prediction block and flight range prediction neural network are designed in this paper according to residual network [30] (ResNet) and dynamic model, by which the predicted flight range can be obtained accurately and quickly. Compared with traditional range calculation methods, the proposed method can greatly improve the speed of range prediction. Aiming at the separation between vehicle's lateral guidance logic and no-fly zone avoidance logic, the concept of no-fly zone crossrange and no-fly zone mapping crossrange are proposed in this paper. And based on the definition of repulsive force in artificial potential field method, an adaptive crossrange corridor is designed, which can avoid no-fly zone and complete lateral guidance under the same guidance logic, and its convergence is also discussed. Compared with traditional lateral guidance methods and no-fly zone avoidance methods, the proposed method can reduce the sign variation numbers of bank angle with the avoidance for the no-fly zones and realized the guarantee of success for the lateral guidance. Finally, through simulation analysis, the suitable block number of the flight range prediction network is determined. And the simulation in different cases show that the proposed method can realize the guidance quickly with less bank angle's sign change under various no-fly zones, and the robustness of the proposed method is also verified through the disturbance experiment.

The innovations of this paper are summarized as follows:

(1) According to the flight range prediction mechanism of reentry glide vehicle, referring to the structure of ResNet, the flight range prediction block and flight range prediction network are designed to realize flight range prediction accurately and quickly

(2) No-fly zone crossrange and no-fly zone mapping crossrange are proposed firstly. By the definition of repulsive force field, an adaptive crossrange corridor is designed to realize the lateral guidance and no-fly zone avoidance of vehicle with less bank angle's sign change. And the convergence of corridor is analyzed theoretically

This paper is arranged as follows. The research status of guidance algorithm of reentry glide vehicle are summarized and innovations are introduced in Section 1. The dynamic model and constraint of reentry glide vehicle are introduced in Section 2. The longitudinal guidance method based on the flight range prediction network is introduced in Section 3. No-fly zone crossrange, no-fly zone mapping crossrange, and lateral guidance logic are introduced, when the convergence of adaptive crossrange corridor are discussed in Section 4. The proposed method is verified by simulation in Section 5. Finally, the summarization of all the work in this paper is in Section 6.

## 2. The Dynamic Model and Constraints of Reentry Glide Vehicle

Without considering the earth's rotation, the dynamic model of the vehicle is shown

$$\begin{cases} \dot{R} = V\sin\theta, \\ \dot{\phi} = \dfrac{V\cos\theta\sin\psi}{(R_e+h)\cos\varphi}, \\ \dot{\varphi} = \dfrac{V\cos\theta\cos\psi}{(R_e+h)}, \\ \dot{V} = -\dfrac{\widehat{D}}{m} - g\sin\theta, \\ \dot{\theta} = \dfrac{\widehat{L}\cos\beta}{mV} + \cos\theta\left(\dfrac{V}{R_e+h} - \dfrac{g}{V}\right), \\ \dot{\psi} = \dfrac{\widehat{L}\sin\beta}{mV\cos\theta} + \dfrac{V\cos\theta\sin\psi\tan\varphi}{R_e+h}, \end{cases} \tag{1}$$

where $H$ is the flight height of vehicle and $\phi$ and $\varphi$ represent the longitude and latitude, respectively. $V$ is the velocity of vehicle and $\theta$ and $\psi$ represent the flight path angle and heading angle, respectively. $\widehat{L}$ and $\widehat{D}$ represent the lift and drag force. $R_e$ represents the radius of earth and $m$ represents the mass of vehicle.

For the convenience of calculation, the nondimensional dynamic model can be described as

$$\begin{cases} \dot{r} = v\sin\theta, \\ \dot{\phi} = \dfrac{v\cos\theta\sin\psi}{r\cos\varphi}, \\ \dot{\varphi} = \dfrac{v\cos\theta\cos\psi}{r}, \\ \dot{v} = -D - \dfrac{\sin\theta}{r^2}, \\ \dot{\theta} = \dfrac{L\cos\beta}{v} + \dfrac{\cos\theta}{v}\left(\dfrac{v^2}{r} - \dfrac{1}{r^2}\right), \\ \dot{\psi} = \dfrac{L\sin\beta}{v\cos\theta} + \dfrac{v\cos\theta\sin\psi\tan\varphi}{r}, \end{cases} \tag{2}$$

where $r$ is the nondimensional geocentric distance, $v$ is the nondimensional velocity, and $L$ and $D$ represent the nondimensional acceleration of lift and drag force, respectively.

$$\begin{cases} L = C_L S\rho v^2 v_c^2/2mg_0, \\ D = C_D S\rho v^2 v_c^2/2mg_0, \end{cases} \tag{3}$$

where $C_L$ is the lift coefficient and $C_D$ is the drag coefficient, $S$ is the stressed area of the vehicle, $m$ is the mass, and $g_0$ is gravitational acceleration at zero altitude. $v_c$ is expressed as $v_c = \sqrt{R_e g_0}$. The energy of vehicle is expressed as $e = 1/r - V^2/2$.

Then there are process constraints, no-fly zone constraints, and terminal constraints in vehicle flight, where terminal constraints is expressed as

$$\begin{cases} r(e_f) = r_f, \\ v(e_f) \geq v_f, \\ \phi(e_f) = \phi_f, \\ \varphi(e_f) = \varphi_f, \end{cases} \tag{4}$$

where $r_f$, $V_f$, $\phi_f$, and $\varphi_f$ represent the terminal radius, velocity, longitude, and latitude, respectively.

The process constraints conclude the heating rate constraint for vehicle $\dot{Q}_{\max}$, dynamic pressure constraint $q_{\max}$, and overload constraint $n_{\max}$. Where $\dot{Q}$, $q$, and $n$ represent the heating rate, dynamic pressure, and overload of vehicle, respectively. $C$ is the aerodynamic heat coefficient. The process constraints can be expressed as

$$\begin{cases} \dot{Q} = C\rho^{0.5}(v \cdot v_c)^{3.15} \leq \dot{Q}_{\max}, \\ q = 0.5\rho(v \cdot v_c)^2 \leq q_{\max}, \\ n = \sqrt{L^2 + D^2}r^2 \leq n_{\max}. \end{cases} \tag{5}$$

In this paper, the no-fly zone is defined as a circular area, where vehicle are not allowed to pass. It can be expressed as

$$\sqrt{(\phi - \phi_b)^2 + (\varphi - \varphi_b)^2} \geq r_b, \tag{6}$$

where $\phi_b$ and $\varphi_b$, respectively, represent the latitude and longitude of no-fly zone's center when $r_b$ is the radius of no-fly zone.

## 3. Design of Longitudinal Guidance

*3.1. Design of Attack Angle Profile.* Considering that the vehicle needs to meet the process constraints, the longitudinal attack angle profile is designed using the attack angle profile of the space shuttle [31], which is shown as follows

$$\alpha = \begin{cases} \alpha_{\max}, & V \geq V_1, \\ \dfrac{\alpha_K - \alpha_{\max}}{V_2 - V_1}(V - V_1) + \alpha_{\max}, & V_2 \leq V < V_1, \\ \alpha_K, & V < V_2, \end{cases} \tag{7}$$

where $V_1 = 5000m/s$, $V_2 = 3000m/s$ in this paper, and $\alpha_K$ represent the attack angle with which the vehicle is in the maximum lift-drag ratio.

*3.2. Bank Angle Corridor.* Transforming the heating rate constraints, dynamic pressure constraints, and overload constraints to the H-V profile, the path constraints can be transform to be the constraints of height as follows

$$\begin{aligned} C\rho_0^{0.5}e^{-((r-1)R_e/2H_0)}(v \cdot v_c)^{3.15} \leq \dot{Q}_{\max} &\longrightarrow r \geq \frac{\left((2H_0)\ln\left(C\rho_0^{0.5}(v \cdot vc)^{3.15}/\dot{Q}_{\max}\right) + R_e\right)}{R_e} = r_{\dot{Q}\ \max}, \\ q = 0.5\rho_0 e^{-((r-1)R_e/H_0)}(v \cdot v_c)^2 \leq q_{\max} &\longrightarrow \frac{\left(H_0 \ln\left(\rho_0(v \cdot vc)^2/(2q_{\max})\right) + R_e\right)}{R_e} = r_{q\ \max}, \\ n = \frac{\rho_0 e^{-((r-1)R_e/H_0)}(v \cdot v_c^2)S\sqrt{C_L^2 + C_D^2}}{2mg_0}r^2 \leq n_{\max} &\longrightarrow r \geq \frac{\left(H_0 \ln\left(\rho_0(v \cdot vc)^2 r^2 S\sqrt{C_L^2 + C_D^2}/2n_{\max}mg_0\right) + R_e\right)}{R_e} = r_{n\ \max}. \end{aligned} \tag{8}$$

Put $r_{\min} = 1 + \max(h_{\dot{Q}\ \max}, h_{q\ \max}, h_{n\ \max})/R_e$ into the quasi-equilibrium glide equation $L\cos\beta + \cos\theta(v^2/r - 1/r^2) \leq 0$, where $\theta \approx 0$ during the flight of the reentry glide vehicle, so the upper boundary of bank angle corridor can be calculated as follows:

$$|\beta|_{c\ \max} = \arccos\frac{\left((1/r_{\min}) - \left(v^2/r_{\min}{}^2\right)\right)}{L_{r\ \min}}. \tag{9}$$

At the same time, the lower boundary of the bank angle corridor can be calculated by using the equilibrium glide equation as follows:

$$|\beta|_{c\ \min} = \arccos\frac{\left((1/r) - \left(v^2/r^2\right)\right)}{L}. \tag{10}$$

The vehicle should meet the constraints $|\beta|_{c\ \min} \leq |\beta| \leq |\beta|_{c\ \max}$ during flight.

*3.3. Intelligent Flight Range Prediction.* For longitudinal guidance of vehicle, in order to make the vehicle having a strong turning ability at the end of flight, the bank angle profile is designed to calculate the amplitude of bank angle in general

$$|\beta| = \beta_0 - \frac{e - e_0}{e - e_f}\left(\beta_f - \beta_0\right), \tag{11}$$

where $\beta_0$ and $\beta_f$ are the amplitude of the initial and terminal bank angle of the vehicle. In general, a lot of predictor-corrector algorithms can also realize effective guidance when $\beta_0 = \beta_f$, in which the bank angle profile is a constant. This paper also selects this setting to verify the validity of the intelligent flight range prediction method.

The bank angle amplitude of predictor-corrector guidance is related to the difference value between the range-to-go $S_{\text{togo}\_f}$ and the predicted flight range $S_p$. Where $S_{\text{togo}\_f} = \arccos[\cos\varphi_f \cos\varphi_p \cos(\phi_f - \phi_p) + \sin\varphi_f \sin\varphi_p]$. In general, the predictor-corrector guidance method obtain the predicted range through integral-iteration method, and its calculation equation is

$$S_p = \int_e^{e_f} \frac{dS_p}{de} de = \int_e^{e_f} \frac{dS_p}{dt}\frac{dt}{de} de = \int_e^{e_f} \frac{\sin\theta}{rD} de \tag{12}$$

Using the numerical discrete integration method (such as Euler method), its calculation process is

$$\begin{aligned} S_p &= \sum_{i=0}^{N} \frac{\cos\theta_i}{r_i D_i}\Delta E = \sum_{i=0}^{N-1}\left(\frac{\cos\theta_i}{r_i D_i} + \frac{\theta_i' \cos\theta_i r_i D_i + \sin\theta_i\left(r_i' D_i + r_i D_i'\right)}{r_i^2 D_i^2}\Delta E\right)\Delta E \\ &= \sum_{i=0}^{N-1}\left(\frac{\cos\theta_i}{r_i D_i}\Delta E + \frac{\sin\theta_i}{r_i D_i^2}\left(\frac{L_i\cos\beta_i}{v_i^2} + \frac{\cos\theta_i}{v_i^2}\left(\frac{v_i^2}{r_i} - \frac{1}{r^2}\right)\right)\Delta E^2\right. \\ &\quad \left. + \frac{\cos\theta_i}{r_i^2 D_i^2}\left(\sin\theta_i - \frac{1}{H_0}\frac{r_i}{v_i} - \frac{D_i}{2r_i} - \frac{\sin\theta_i}{2r_i^3}\right)\Delta E^2\right) \end{aligned} \tag{13}$$

where $\Delta E = (e_f - e)/N$, $N$ represents the number of iteration steps, $\theta' = d\theta/de$, $r' = dr/de$, and $D' = dD/de$.

It can be seen that the influencing factors of flight range prediction are state $r_i, v_i, \theta_i$ and bank angle $\beta_i$ at each time. The state of the vehicle at each time $r_i, v_i, \theta_i$ is related to the initial state $r_0, v_0, \theta_0$ and the bank angle at each time $\beta_0, \cdots, \beta_i$. In order to improve the accuracy of flight range prediction, the same corridor constraint for guidance should be added in iteration. The predicted flight range of different initial states under different bank angles are shown in Figure 1.

It can be seen that due to the existence of bank angle corridor, the predicted flight range in different initial states show continuous nonlinear characteristics under the same bank angle, and three-dimensional function relationship is not obvious. The function relationship between the predicted flight range and initial state $r_0, v_0, \theta_0$ is shown in Figures 2(a)–2(c) under the same bank angle. In Figures 2(a)–2(c), the vehicle's bank angle is $\beta_0 = 38°$; case 1, 2, and 3 represent different initial states, respectively, and the information is shown in Table 1.

It can be seen from Figures 2(a) and 2(c) that the initial flight path angle of vehicle has almost no impact on the predicted flight range under bank angle corridor when it has a small impact at high speed. As can be seen from Figure 2(b), the predicted flight range of vehicle is proportional to the speed. And with the same speed and flight path angle, the largest predicted flight range is not a simple proportional relationship with height. There exist a peak in the curve when the initial velocity increases with the peak's height higher. It is

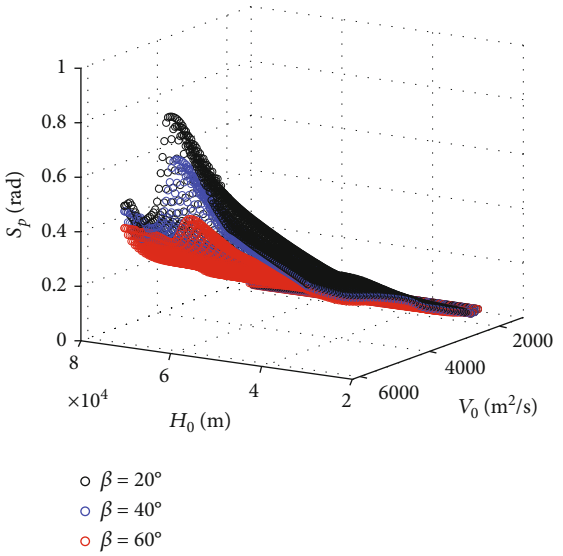


Figure 1: Relationship between predicted flight range and initial state under different bank angle.

due to the bank angle corridor under which the initial bank angle of vehicle at high speed at high height has to be adjusted. On the whole, there is a highly coupled nonlinear relationship among vehicle's predicted flight range, initial state, and bank angle, which is difficult to be fitted effectively by nonlinear function or simple multilayer perceptron (MLP). To solve this problem, based on the integral-iteration process of flight range prediction and the structure of ResNet, the flight range prediction block and flight range prediction neural network are designed to realize flight range prediction effectively. Its structure is shown in Figure 3.

As seen from Figure 3(a), the structure of flight range prediction block is same as Equation (13), which can regard one flight range prediction block as a step of the integral-iteration process. It includes two layers of fully connected network and Relu activation function to simulate differential of the state $\dot{r}_i, \dot{v}_i, \dot{\theta}_i$ and change rate of bank angle $\dot{\beta}$ between two points of flight. And differential of predicted flight range $\dot{S}_{pi}$ is added into the output of block, which satisfies $\dot{S}_{pi}\Delta E = \int_{e_i}^{e_{i+1}} \dot{S}_p de = \Delta S_{pi}$. Then take the sum of $\Delta S_{pi}$ as shown in Figure 3(b), the predicted flight range can be obtained. On the other hand, due to structure of block is similar as the ResNet's base block, the input of the block can be added into output directly, which can reduce the gradient diffusion and disappear caused by the deep network. In this way, the flight range neural network can also be training effectively when layers number of network reaches one hundred and more.

For traditional predictor-corrector guidance methods, the bank angle $\beta_0$ is usually calculated through secant method, which satisfies $f(\beta_0) = 0$. It can be expressed as

$$\beta_0(i+1) = \beta_0(i) - a_i \frac{\beta_0(i) - \beta_0(i-1)}{f_i - f_{i-1}} f_i, \tag{14}$$

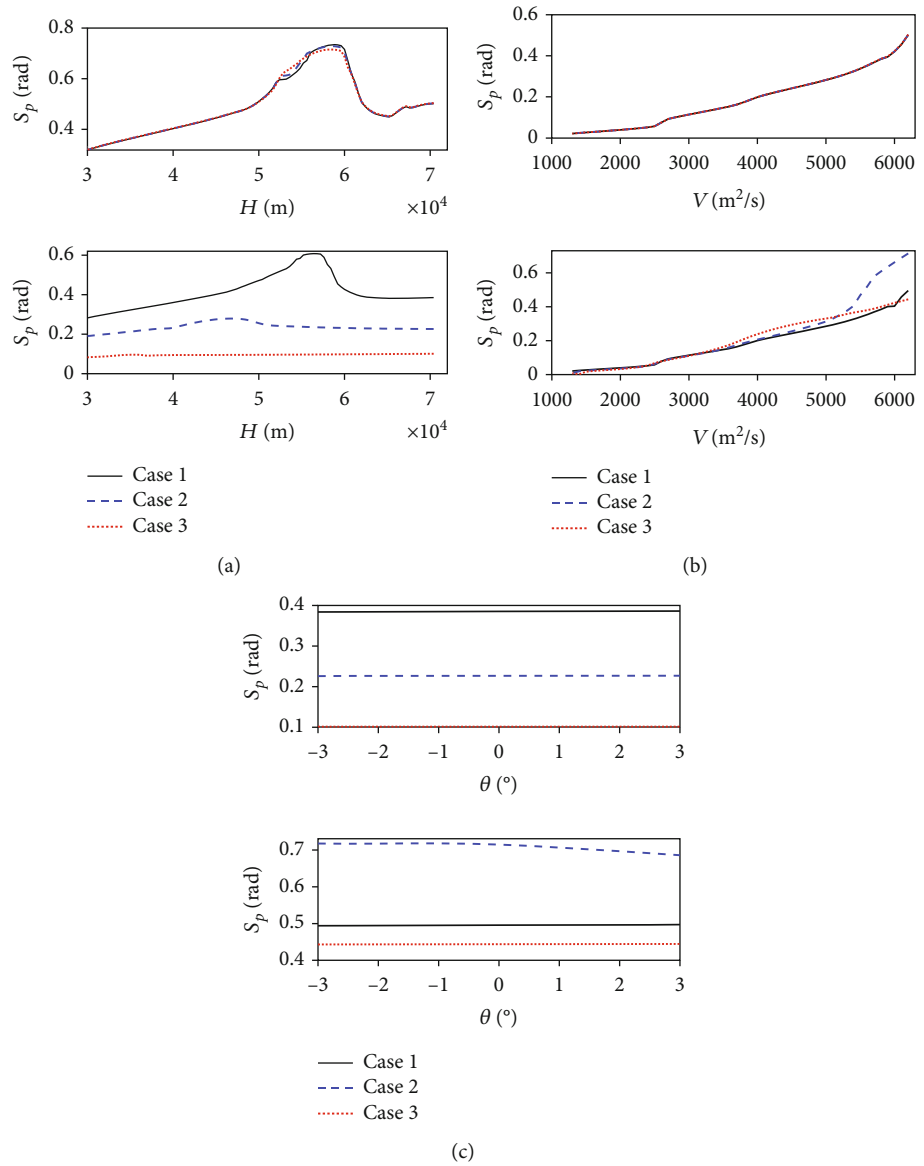


Figure 2: Relationship between the initial state with the predicted flight range. (a) is the relation between the height and the predicted flight range. (b) is the relation between the speed and the predicted flight range. (c) is the relation between the flight path angle and predicted flight range.

where $a_i$ is the adjustment coefficient and $f_i$ is the difference valve between predicted flight range and range-to-go of $i$-th iteration.

The convergence speed of the traditional secant method is easily affected by the initial value and the adjustment coefficient. In this paper, when the network is used for calculating $\beta_0$, the different initial bank angle in the same state are inputted into flight range prediction network as a batch and make use of $S_f$ by inverse interpolation solution function to obtain $\beta_0$ which satisfies $f = 0$. Assuming flight range prediction network as $f_p(\cdot)$, and the inverse interpolation solution function can expressed as $I_p(\cdot)$. $\beta_0$ can be calculated as

$$\beta_0 = I_p\left(f\left(S, \beta_{1,..,N}\right), S_{\text{togo\_}f}\right) = I_p\left(S_{p1,\cdots,p_N}, S_{\text{togo\_}f}\right). \quad (15)$$

The time complexity of traditional predictor-corrector guidance method is $O(n^2)$, in which the integral flight range prediction method and secant method. Through the method in this paper, the flight range prediction network replaces the iterative process of interval range prediction, by which the time complexity is $O(1)$. And through the inverse interpolation solution method, the time complexity is also reduced to $O(1)$ compared with the secant method. The time complexity of the proposed algorithm for calculating the value of bank angle is $O(1)$.

## 4. Design of Lateral Guidance Method

In the common design of lateral guidance law, the lateral guidance effect of vehicle is more easily reflected by the crossrange corridor compared with the heading deviation angle corridor.

Table 1: Initial state of case.

| Figure | Case 1 | Case 2 | Case 3 |
|---|---|---|---|
| (a) up | $V_0 = 6200\ m/s$, $\theta_0 = -3^o$ | $V_0 = 6200\ m/s$, $\theta_0 = -1^o$ | $V_0 = 6200\ m/s$, $\theta_0 = -1^o$ |
| (a) down | $V_0 = 5800\ m/s$, $\theta_0 = 0^o$ | $V_0 = 4300 m/s$, $\theta_0 = 0^o$ | $V_0 = 2800 m/s$, $\theta_0 = 0^o$ |
| (b) up | $H_0 = 70.4$km, $\theta_0 = -3^o$ | $H_0 = 70.4$ km, $\theta_0 = -1^o$ | $H_0 = 70.4$ km, $\theta_0 = -1^o$ |
| (b) down | $H_0 = 68.8$ km, $\theta_0 = 0^o$ | $H_0 = 56.8$ km, $\theta_0 = 0^o$ | $H_0 = 44.8$km, $\theta_0 = 0^o$ |
| (c) up | $H_0 = 70.4$ km, $V_0 = 5800\ m/s$ | $H_0 = 70.4$ km, $V_0 = 4300\ m/s$ | $H_0 = 70.4$ km, $V_0 = 2800 m/s$, |
| (c) down | $H_0 = 68.8$ km, $V_0 = 6200 m/s$ | $H_0 = 56.8$ km, $V_0 = 6200 m/s$ | $H_0 = 46.8$km, $V_0 = 6200 m/s$ |

What is more, the avoidance logic of no-fly zone and crossrange corridor guidance logic are often separate, and the convergence condition of crossrange is not considered in the design of dynamic corridor. To solve this problem, no-fly zone crossrange and no-fly zone mapping crossrange are proposed based on definition of crossrange and artificial potential field. On this basis, an adaptive crossrange corridor combining no-fly zone avoidance and lateral guidance is designed, and its convergence is analyzed.

*4.1. No-Fly Zone Crossrange and No-Fly Zone Mapping Crossrange.* Crossrange of vehicle is the distance between the vehicle's velocity and the terminal position, it can be expressed as

$$\chi = \arcsin\left(\sin\left(S_{\text{togo}\_f}\right)\sin\left(\Delta\psi_f\right)\right), \tag{16}$$

where $\Delta\psi_f$ is the heading deviation angle between vehicle and terminal position. $\Delta\psi_f = \psi - \psi_f$, and $\psi_f$ is the sight line angle between vehicle and terminal position, which can be expressed as

$$\psi_f = \arcsin\frac{\sin\left(\phi_f - \phi\right)\cos\varphi_f}{\sin\left(S_{\text{togo}\_f}\right)}. \tag{17}$$

Based on the definition of crossrange, the concept of no-fly zone crossrange and no-fly zone mapping crossrange are proposed as shown in Figure 4.

As shown in Figure 4(a), no-fly zone crossrange represents the distance between the center of no-fly zone and the velocity direction of vehicle. The definition can expressed as

$$\chi_b = \begin{cases} \arcsin\left(\sin\left(S_b\right)\sin\left(\Delta\psi_b\right)\right), & \text{if } |\Delta\psi_b| < \dfrac{\pi}{2}, \\ \infty, & \text{if } |\Delta\psi_b| \geq \dfrac{\pi}{2}, \end{cases} \tag{18}$$

where $S_b = \arccos\left(\cos\varphi\cos\varphi_b\cos\left(\phi - \phi_b\right) + \sin\varphi\sin\varphi_b\right)$, which is the distance between center of no-fly zone and vehicle. $\psi_b = \arcsin\left(\sin\left(\phi_b - \phi\right)\cos\varphi/\sin\left(S_b\right)\right)$, which represents the sight line angle between center of no-fly zone and vehicle. $\Delta\psi_b = \psi - \psi_b$. The sight line angles of the no-fly zone boundaries are $\psi_{b\ \min}$, $\psi_{b\ \max}$, which can be expressed as

$$\begin{aligned} \psi_{b\ \max} &= \psi_b + arc\sin\frac{r_b}{S_b}, \\ \psi_{b\ \min} &= \psi_b - arc\sin\frac{r_b}{S_b}. \end{aligned} \tag{19}$$

No-fly zone mapping crossrange represents the mapping distance on the vehicle's crossrange cause of no-fly zone, which is shown in Figure 4(b). The basic crossrange corridor $\chi_{0\ \max}$ and $\chi_{0\ \min}$ in this paper can be expressed as

$$\begin{aligned} \chi_{0\ \max} &= \arcsin\left(\sin\left(S_{\text{togo}\_f}\right)\sin\left(\left(\frac{\pi}{18}\right)\frac{S_{\text{togo}\_f}}{S_{\text{togo}\_f0}} + \frac{\pi}{36}\right)\right), \\ \chi_{0\ \min} &= -\arcsin\left(\sin\left(S_{\text{togo}\_f}\right)\sin\left(\left(\frac{\pi}{18}\right)\frac{S_{\text{togo}\_f}}{S_{\text{togo}\_f0}} + \frac{\pi}{36}\right)\right), \end{aligned} \tag{20}$$

where $S_{\text{togo}\_f0}$ is the range-to-go at the initial time.

And the lower boundary and upper value boundary of no-fly zone mapping crossrange $\chi_{b\ \min}$ and $\chi_{b\ \max}$ can be calculated as

$$\begin{aligned} \chi_{b\ \min} &= \arcsin\left(\sin\left(S_{\text{togo}\_f}\right)\sin\left(\psi_{b\ \min} - \psi_f\right)\right), \\ \chi_{b\ \max} &= \arcsin\left(\sin\left(S_{\text{togo}\_f}\right)\sin\left(\psi_{b\ \max} - \psi_f\right)\right). \end{aligned} \tag{21}$$

The mapping crossrange is calculated as Equation (22), which is the overlap crossrange between basic crossrange corridor and the mapping area's no-fly zone crossrange.

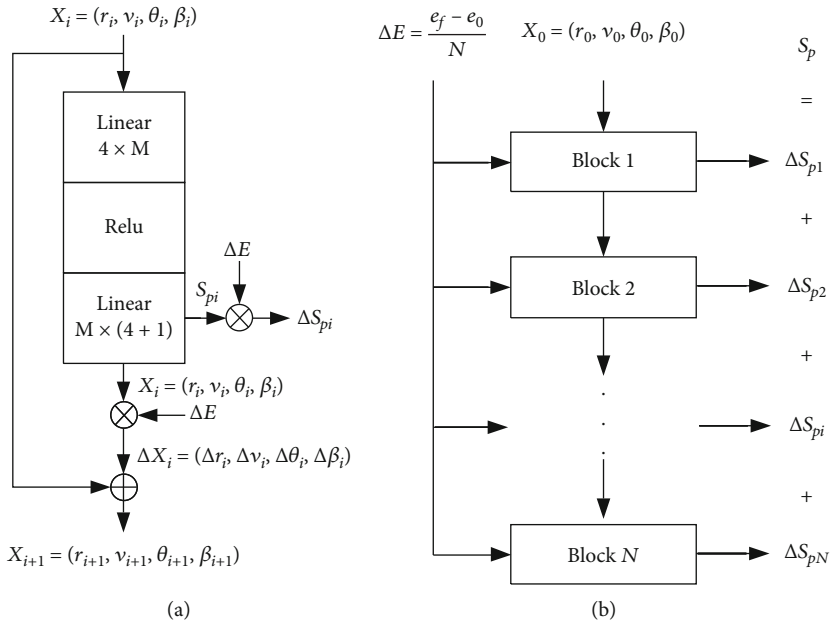


FIGURE 3: Design of flight range block and flight range neural network. (a) is the structure of the flight range prediction block. (b) is the structure of the flight range prediction neural network.

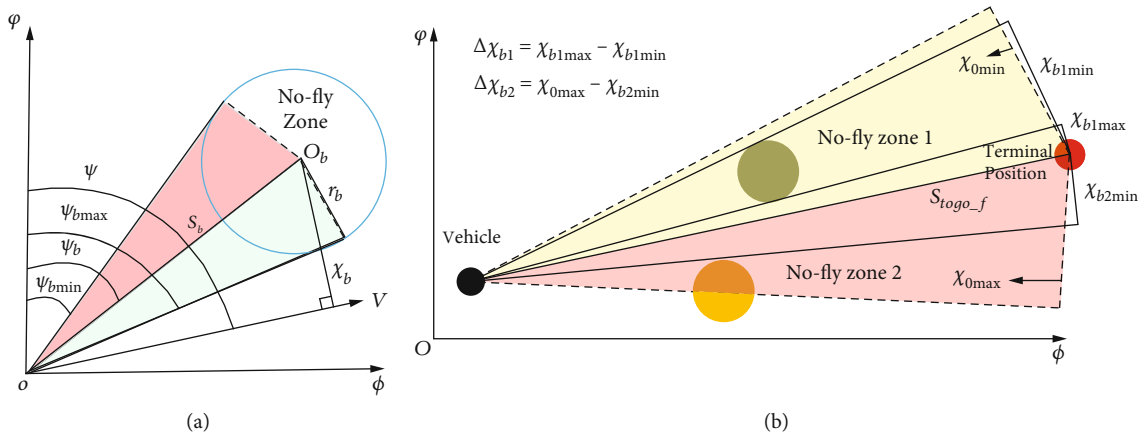


FIGURE 4: No-fly zone crossrange and no-fly zone mapping crossrange. (a) represents the no-fly zone crossrange. (b) represents the no-fly zone mapping crossrange.

$$\Delta\chi_b = \begin{cases} 0, & \text{if } \chi_{b\ \max} < \chi_{0\ \min}, \\ \min\left(\chi_{b\ \max}, \chi_{0\ \max}\right) - \max\left(\chi_{b\ \min}, \chi_{0\ \min}\right), \\ 0, & \text{if } \chi_{b\ \min} > \chi_{0\ \max}. \end{cases} \tag{22}$$

*4.2. Adaptive Crossrange Corridor.* According to the concept of repulsive force in artificial potential field, an adaptive crossrange corridor for reentry glide vehicle is designed, in which the boundary can be adjusted adaptively. And the sign of no-fly zone crossrange represents the direction of the repulsive force, the value of no-fly zone crossrange and distance between center of no-fly zone and vehicle decide the weight of repulsive force, which can be expressed as

$$\phi_s(S_{\text{bi}}, r_{\text{bi}}) = \begin{cases} \dfrac{1}{\left(S_{\text{bi}} - n_i r_{\text{bi}} + 1\right)^2}, & \text{if } S_{\text{bi}} > n_i r_{\text{bi}}, \\ 1, & \text{if } S_{\text{bi}} < n_i r_{\text{bi}}, \end{cases} \tag{23}$$

$$\phi_\chi(\chi_{\text{bi}}, r_{\text{bi}}) = \begin{cases} \dfrac{r_b^2}{\left(|\chi_{\text{bi}}|\right)^2}, & \text{if } \chi_{\text{bi}} > r_{\text{bi}}, \\ 1, & \text{if } \chi_{\text{bi}} < r_{\text{bi}}, \end{cases} \tag{24}$$

where $\phi_s$ represents the weight relate to distance between the no-fly zone and vehicle and $\phi_\chi$ represents the weight relate to

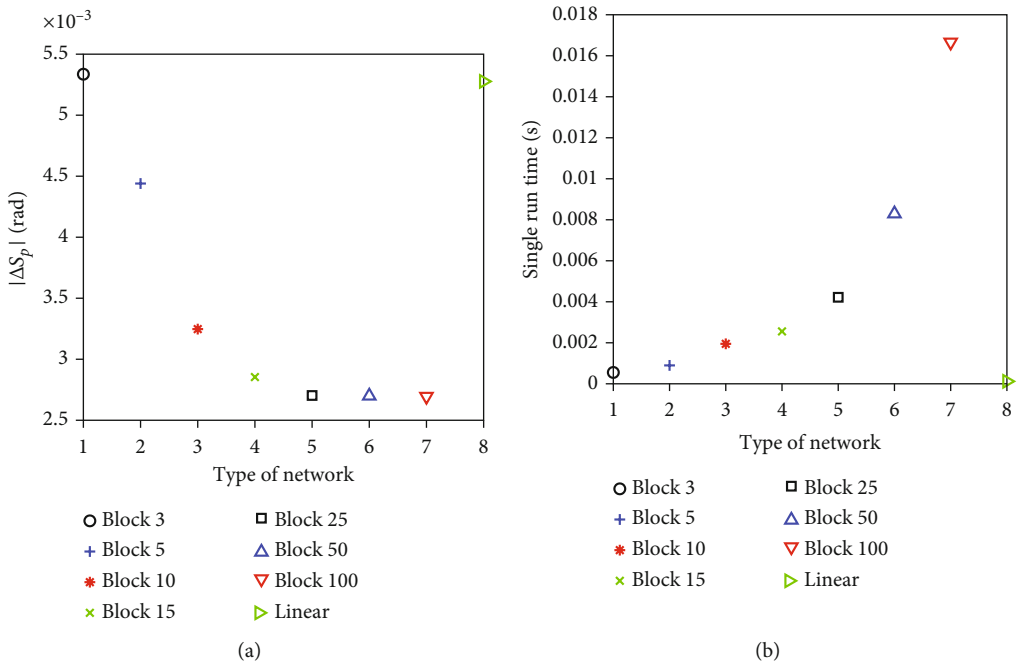


Figure 5: The result of flight range prediction network. (a) is the result of the predicted flight range with different blocks number. (b) is the result of the single running time with different blocks number.

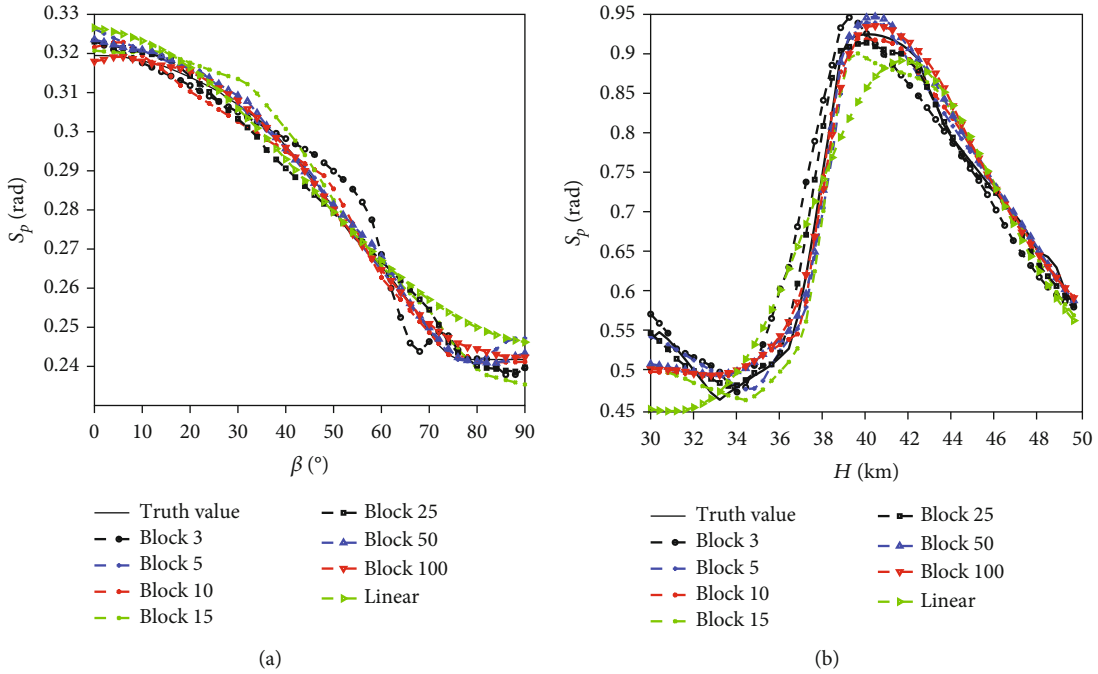


Figure 6: Comparison of flight range prediction result. (a) is the predicted range with different bank angle. (b) is the predicted range with different initial state.

no-fly zone crossrange. $n_i$ represents the impact factors of the no-fly zone of $i$-th no-fly zone, and the value is larger when the no-fly zone's initial distance is greater in order to combine the effects of multiple no-fly zones.

Equations (23) and (24) mean that the repulsive force will decrease quickly when the distance between vehicle and no-fly zone is out of setting range; the repulsive force will also decrease quickly when the velocity direction is not going through the no-fly zone.

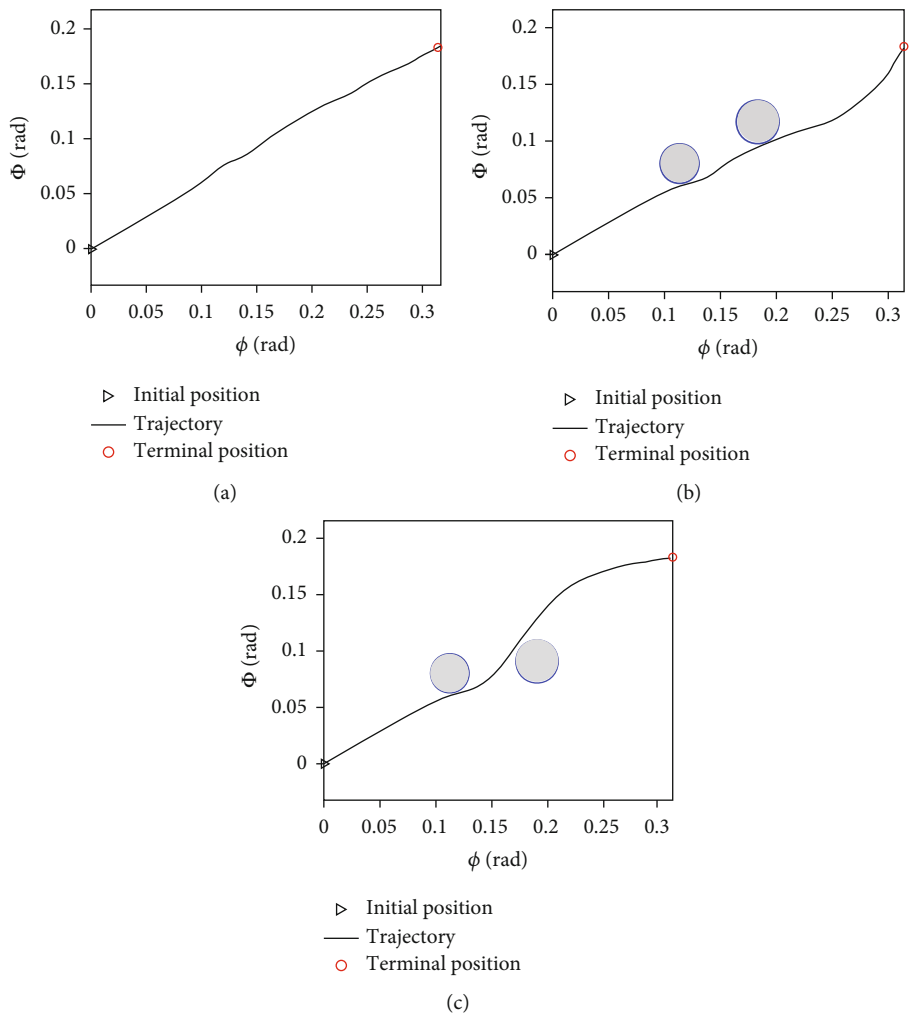


Figure 7: Lateral guidance trajectory. (a) is the generated trajectory in the Case 1. (b) is the generated trajectory in the Case 2. (c) is the generated trajectory in the Case 3.

Then, assuming that the truth upper and lower boundary of the crossrange corridor at $t$-th time are $\chi_{t\ \max}$ and $\chi_{t\ \min}$, and the theoretical boundaries are $\bar{\chi}_{t\ \max}$ and $\bar{\chi}_{t\ \min}$, the change law of crossrange corridor's upper and lower boundary can be expressed as

$$\begin{aligned}
\bar{\chi}_{t\ \max} &= \chi_{t0\ \max} + \sum_{i}^{n} \operatorname{sign}(\chi_{\mathrm{tbi}})\phi_{\mathrm{tbi}}\phi_{t\chi i}\Delta\chi, \\
\chi_{t\ \max} &= \chi_{t-1_\max} + \operatorname{sgn}\left(\bar{\chi}_{t\ \max} - \chi_{t-1\ \max}\right) \min\left(|\dot{\chi}_{t-1}|\Delta t, |\bar{\chi}_{t_\max} - \chi_{t-1_\max}|\right), \\
\bar{\chi}_{t\ \min} &= \chi_{t0\ \min} + \sum_{i}^{n} \operatorname{sgn}(\chi_{\mathrm{tbi}})\phi_{\mathrm{tbi}}\phi_{t\chi i}\Delta\chi_{\mathrm{tb}}, \\
\chi_{t\ \min} &= \chi_{t-1_\min} + \operatorname{sgn}\left(\bar{\chi}_{t_\min} - \chi_{t-1_\min}\right) \min\left(|\dot{\chi}|\Delta t, |\bar{\chi}_{t_\min} - \chi_{t-1_\min}|\right).
\end{aligned} \tag{25}$$

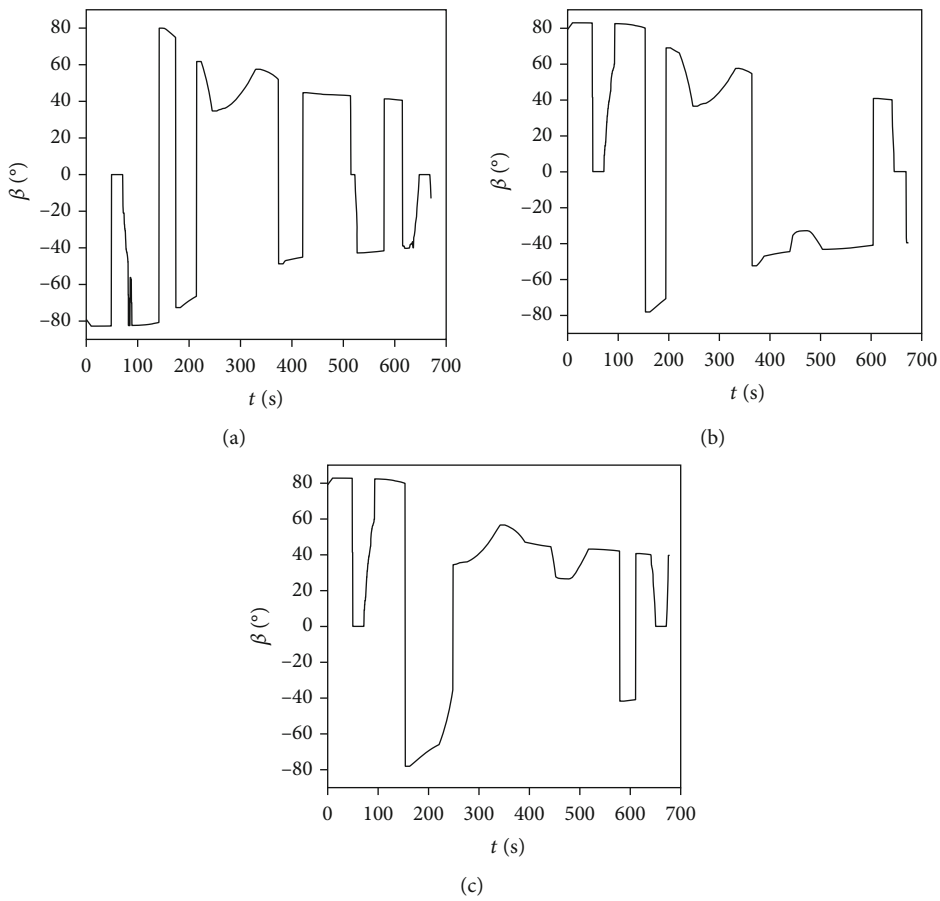


Figure 8: Variation of bank angle. (a) is the variation of the bank angle in the Case 1. (b) is the variation of the bank angle in the Case 2. (c) is the variation of the bank angle in the Case 3.

The change logic of bank angle's sign can be express as

$$\begin{cases} \operatorname{sgn}(\beta_t) = 1 & \text{if } \chi_t = \chi_{t\ \min}, \\ \operatorname{sgn}(\beta_t) = -1 & \text{if } \chi_t = \chi_{t\ \min}, \\ \operatorname{sgn}(\beta_t) = \operatorname{sgn}(\beta_{t-1}) & \text{if } \chi_{t\ \min} \le \chi_t \le \chi_{t\ \max}. \end{cases} \tag{26}$$

### 4.3. Convergence Analysis of Lateral Guidance Method

**Lemma 1.** *Under the change logic of bank angle's sign in this paper, if* $\chi_{0\ \min} \le \chi_0 \le \chi_{0\ \max}$ *and* $|\dot{\chi}_{\min}(t)| \le |\dot{\chi}(t)|, |\dot{\chi}_{\max}(t)| \le |\dot{\chi}(t)|$, *then* $\chi_{\min}(t) \le \chi(t) \le \chi_{\max}(t)$

*Proof.* $\because \chi_{0\ \min} \le \chi_0 \le \chi_{0\ \max}$

Let $\operatorname{sgn}(\beta_0) = 1$

$,\exists \varepsilon_{t0}, \chi_{\max}(\varepsilon_{t0}) = \chi(\varepsilon_{t0}), \operatorname{sgn}(\beta(\varepsilon_{t0})) = -1$

Then $\because |\dot{\chi}_{\min}(t)| \le |\dot{\chi}(t)|, |\dot{\chi}_{\max}(t)| \le |\dot{\chi}(t)|$

$$\therefore |\dot{\chi}_{\max}(\varepsilon_{t0})| \le |\dot{\chi}(\varepsilon_{t0})|, \tag{27}$$

If $\chi_{\max}(\xi_{t0}) - \chi_{\min}(\xi_{t0}) > 0, \exists \varepsilon_t > 0, \chi_{\min}(t) \le \chi_0(t) \le \chi_{0\ \max}(t), \varepsilon_{t0} \le t \le \varepsilon_t$

$$\therefore \chi_{\min}(t) \le \chi_0(t) \le \chi_{0\ \max}(t) \tag{28}$$

According to the design of corridor, $\chi_{t\ \max} \longrightarrow \bar{\chi}_{t\ \max}$, $\chi_{t\ \min} \longrightarrow \bar{\chi}_{t\ \min}$ after the vehicle realizing avoidance of no-fly zone. And $\bar{\chi}_{t\ \max} = \chi_{0\ \max}, \bar{\chi}_{t\ \min} = \chi_{0\ \min,}$ so $\lim_{t \longrightarrow t_f} \chi_{t\ \max} = 0, \lim_{t \longrightarrow t_f} \chi_{t\ \min} = 0$. And according to Lemma 1, $\chi_{\min}(t) \le \chi(t) \le \chi_{\max}(t)$, so $\lim_{t \longrightarrow t_f} \chi = 0$. □

## 5. Simulation

### 5.1. Setting of Simulation and Training

*5.1.1. Simulation Environment.* In simulation, CAV-H is selected as the object, whose key parameters can refer to literature [32]. The guidance interval is 0.3 s. PC CPU selects Inter-i7, and GPU selects GTX 2080ti, MATLAB is selected to generate the train data set of flight range prediction network and draw the simulation results when PyTorch and Python are selected to train networks and realize guidance.

*5.1.2. Data Set and Training Setting.* The data set for the flight range prediction network is generated by integral-iteration method with bank angle corridor, in which vehicle's initial height is within 30 to 70.4 km, and initial speed is within 1500 to 6200 m/s, and the initial bank angle is within -3 to 3°. All the initial state satisfy uniform distribution. During

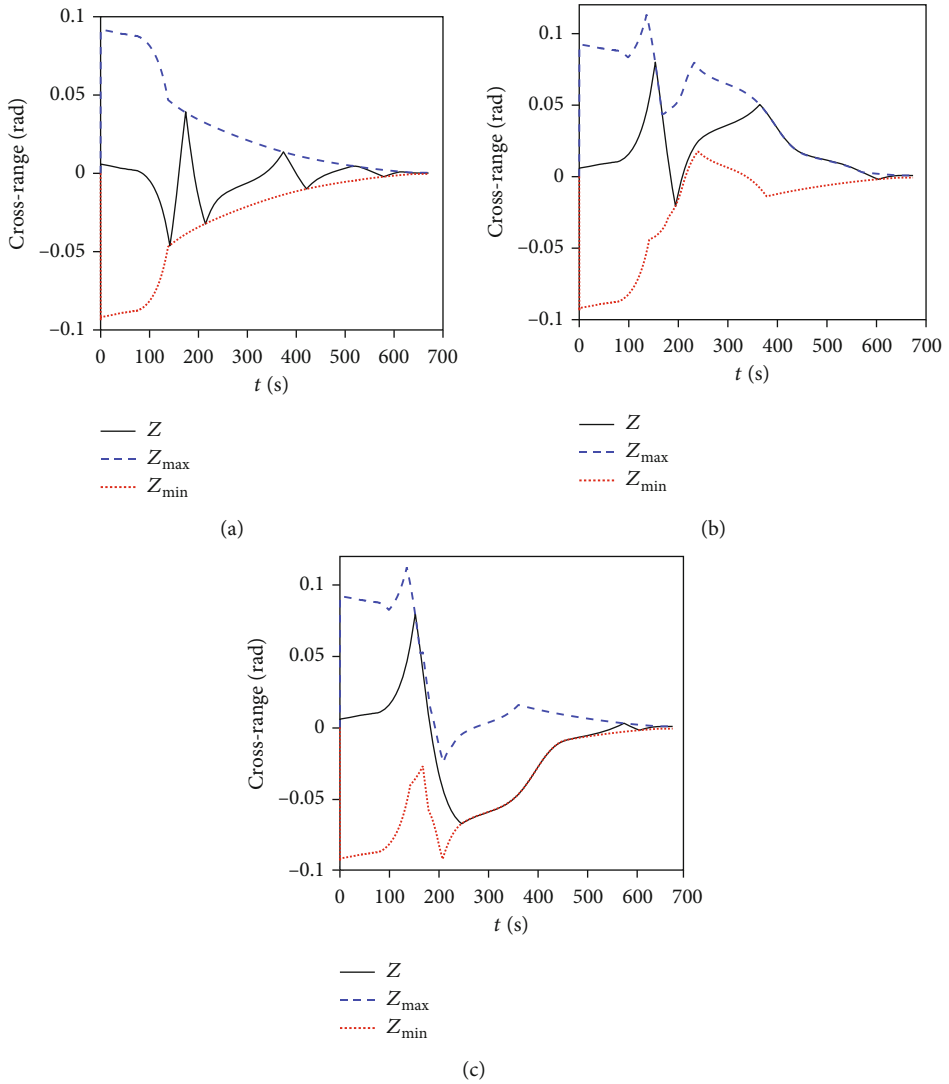


Figure 9: Variation of the crossrange and crossrange corridor. (a) is the variation of the crossrange in the Case 1. (b) is the variation of the crossrange in the Case 2. (c) is the variation of the crossrange in the Case 3.

training, 4/5 of datasets are selected as train set and 1/5 of datasets are selected as test set.

In the training process, the MSE loss are selected as the loss function, Adam optimizer is selected when the learning rate is equal to $5e-4$. A train batch includes 10,000 samples and network is trained 2,000 epochs.

### 5.2. Analysis of Simulation Results

*5.2.1. Effect Analysis of Flight Range Prediction Network.* In this paper, the simulation results of the flight range prediction network is analyzed, which includes 3, 5, 10, 15, 25, 50, and 100 blocks, when the result is also compared with that of pure fully connected network. The average prediction error of test data set and the running time of each network are shown in Figure 5. It can be seen from Figure 5(a) that as the number of blocks increases, prediction error becomes smaller and smaller. This is because the more prediction blocks there are, the more the network prediction process is closer to the iterative process with lower energy interval, which can improve accuracy of prediction. On the other hand, compared with pure fully connected network, flight range prediction network has more accurate prediction result, which is due to its network structure closer to the original dynamic model. As can be seen from Figure 5(b), with the gradual increase of prediction blocks, the single running time of the network increases gradually. This is because the deeper the

Table 2: Simulation results of cases.

| Case | $\Delta\phi_f(^\circ)$ | $\Delta\varphi_f(^\circ)$ | $\Delta h_f(km)$ | $\chi_f(^\circ)$ | $E$(km) |
|---|---|---|---|---|---|
| 1 | -0.017 | 0.017 | -1.863 | -0.021 | 3.233 |
| 2 | -0.009 | 0.034 | -1.823 | -0.014 | 4.340 |
| 3 | $7.7e-4$ | -0.006 | -1.724 | 0.010 | 2.188 |

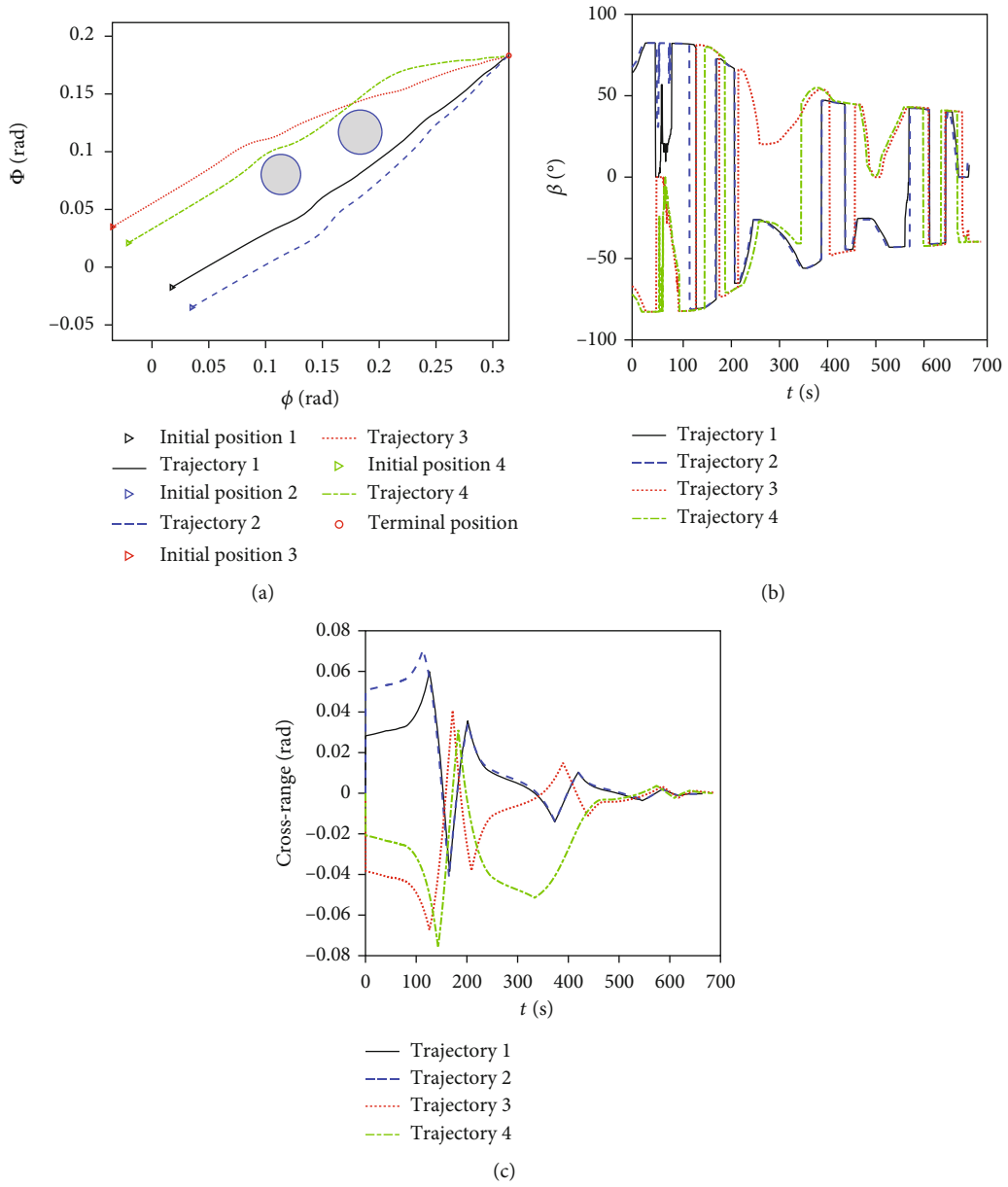


FIGURE 10: Simulation result of guidance with different initial position. (a) is the lateral trajectories of the vehicle. (b) is the variation of the bank angle. (c) is the variation of the crossrange.

network is, the more parameters it has, the more operations it needs to carry out, which will affect the running time.

The prediction results with initial state $(H_0 = 38\text{km}, V_0 = 5300m/s, \theta_0 = 0^\circ)$ under different bank angle and the prediction results with the state $(H_0 = 50.8\text{-}70.4\text{km}, V_0 = 5300\ m/s, \theta_0 = 0^\circ)$ when bank angle is equal to 0 are shown in Figure 6. As can be seen from Figure 6(a), when the number of prediction block increases, the fitting effect of the network gets better and smoother. Compared with the fully connected network, the prediction network's fitting precision is higher and more consistent with the vehicle's change. As can be seen from Figure 6(b), as the initial state changes, there is a large error between the predicted flight range and the truth value. However, as the number of prediction block increases, the predicted result of flight range prediction network becomes more and more accurate. Both speed and accuracy of prediction are considered, the network structure with 25 blocks is selected to obtain predicted flight range in this paper.

*5.2.2. Analyzing for the Validity of Algorithm.* The guidance results for three representative cases are analyzed firstly. There is no no-fly zone in case 1, which is shown that the guidance algorithm can work well under general conditions. And case 2 is shown that if vehicle can realize guidance with avoidance of two consecutive no-fly zones when case 3 is shown that if vehicle can realize guidance with going through between two no-fly zones. The initial state of vehicle $(\phi_0, \varphi_0, h_0, V_0, \theta_0, \psi_0)$ is $(0^\circ, 0^\circ, 70\text{km}, 6000m/s, 0.1^\circ, 60^\circ)$,

Table 3: Simulation results of vehicle with different initial position.

| Trajectory | $\phi_0(^\circ)$ | $\varphi_0(^\circ)$ | $\Delta\phi_f(^\circ)$ | $\Delta\varphi_f(^\circ)$ | $\Delta h_f(km)$ | $\chi_f(^\circ)$ | $E$(km) | $F$ |
|---|---|---|---|---|---|---|---|---|
| 1 | 1 | -1 | 0.025 | 0.006 | -0.612 | 0.009 | 2.976 | 9 |
| 2 | 2 | -2 | -0.034 | -0.017 | -0.642 | -0.009 | 4.340 | 9 |
| 3 | -2 | 2 | -0.024 | 0.008 | -1.864 | -0.014 | 3.361 | 8 |
| 4 | -1.2 | 1.2 | 0.059 | 3.8e-5 | -1.880 | -0.014 | 1.830 | 7 |

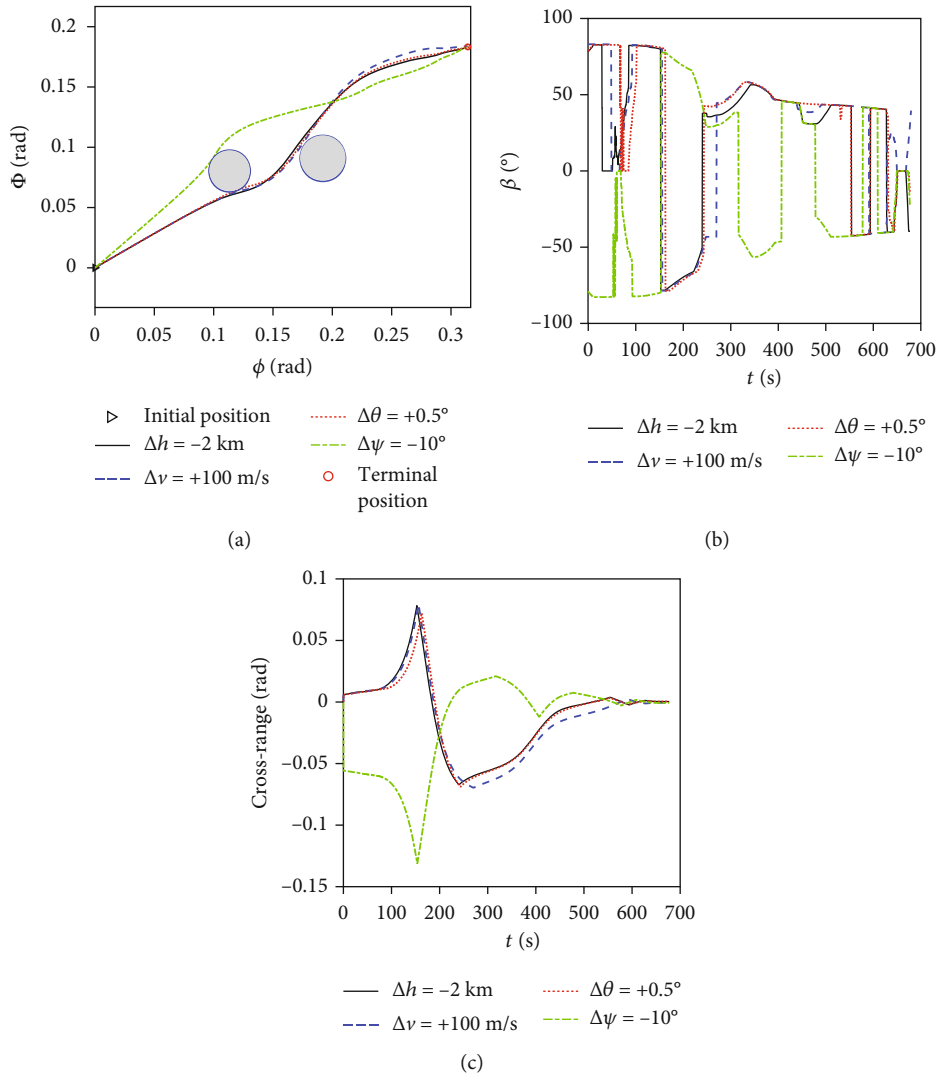


Figure 11: Simulation result of guidance with different initial state. (a) is the lateral trajectories of the vehicle. (b) is the variation of the bank angle. (c) is the variation of the crossrange.

when the terminal state $(\phi_f, \varphi_f, h_f, V_f)$ is $(18^\circ, 10.5^\circ, 30\text{km}, 1500m/s)$. And the no-fly zone information is

Case 2: $(\phi_{b1}, \varphi_{b1}, r_{b1}) = (6.5^\circ, 4.6^\circ, 1^\circ)$, $(\phi_{b2}, \varphi_{b2}, r_{b2}) = (10.5^\circ, 6.7^\circ, 1.1^\circ)$.

Case 3: $(\phi_{b1}, \varphi_{b1}, r_{b1}) = (6.5^\circ, 4.6^\circ, 1^\circ)$, $(\phi_{b2}, \varphi_{b2}, r_{b2}) = (11^\circ, 5.2^\circ, 1.1^\circ)$.

where $\phi_{bi}, \varphi_{bi}, r_{bi}$ represent the center's longitude, latitude of the $i$-th no-fly zone, and the radius of the $i$-th no-fly zone. And the $n_1, n_2$ in Equation (24) are selected $(2, 3.5)$.

The lateral guidance results of case 1, 2, and 3 are shown in Figure 7. It can be seen from case 1 that vehicle can reach the terminal position finally with curvature changes. It can be seen from case 2 to case 3 that vehicle can realize guidance when the no-fly zones are avoided validly.

The variation of bank angle are shown in Figure 8 when variation of crossrange and crossrange corridor are shown in Figure 9. As can be seen from Figures 8(a)–9(a), when there is no-fly zone, vehicle can reach the target position through several

Table 4: Simulation results with initial disturbed state.

| Trajectory | $\Delta\phi_f(^\circ)$ | $\Delta\varphi_f(^\circ)$ | $\Delta h_f(km)$ | $\chi_f(^\circ)$ | $E$(km) | $F$ |
|---|---|---|---|---|---|---|
| $\Delta h_0 = -2km$ | -0.035 | -0.018 | -0.746 | 0.023 | 4.676 | 6 |
| $\Delta v_0 = +100m/s$ | 0.045 | 0.001 | -0.301 | -0.013 | 5.023 | 6 |
| $\Delta\theta_0 = +0.5^o$ | -0.037 | -0.013 | -0.632 | -0.001 | 4.535 | 6 |
| $\Delta\psi_0 = -10^o$ | -0.062 | -0.020 | -0.916 | -0.014 | 6.532 | 7 |

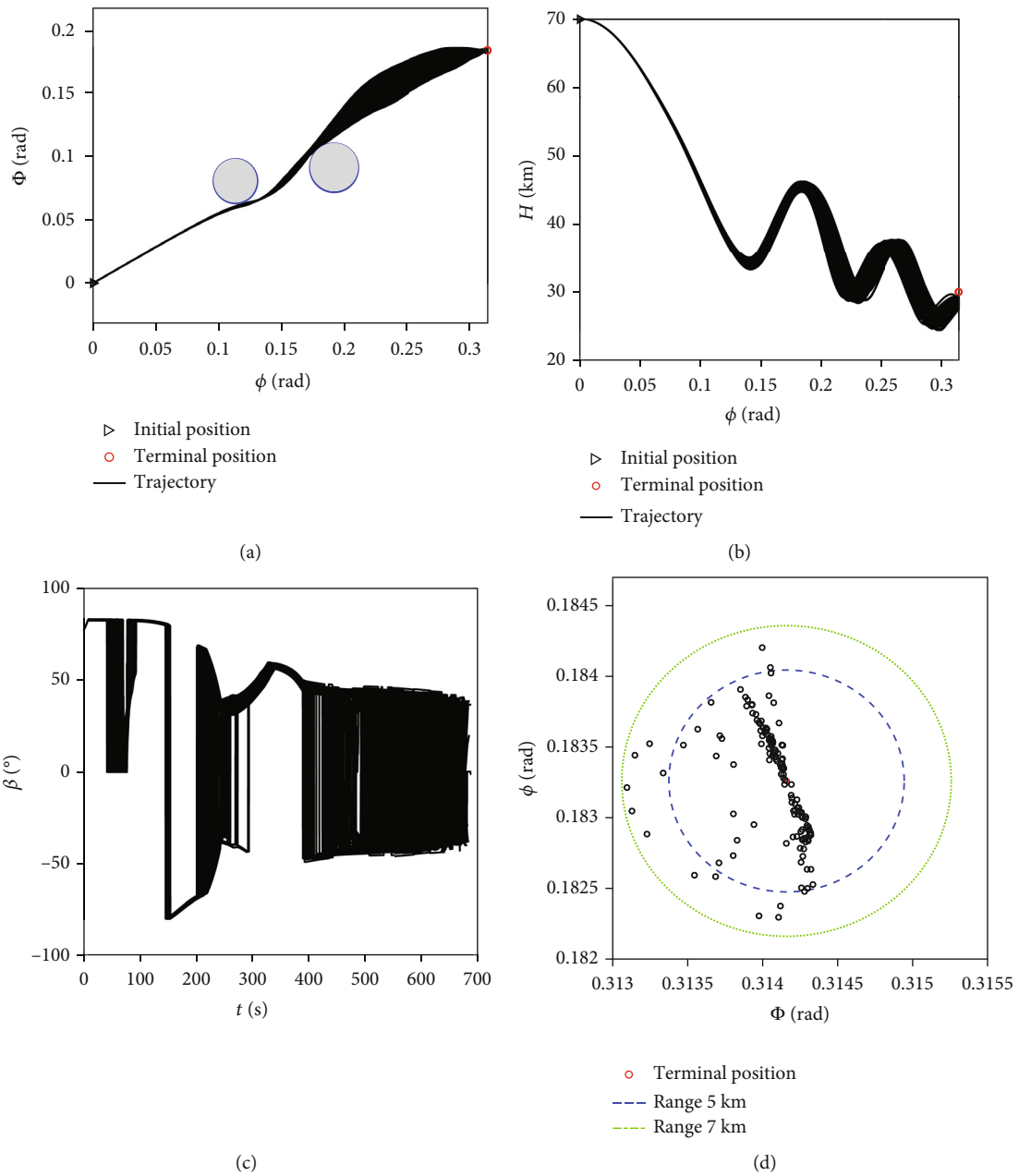


Figure 12: Guidance result with disturbed reentry process. (a) is the lateral trajectories of the vehicle. (b) is the longitudinal trajectories of the vehicle. (c) is the variation of the bank angle. (d) is the variation of the crossrange.

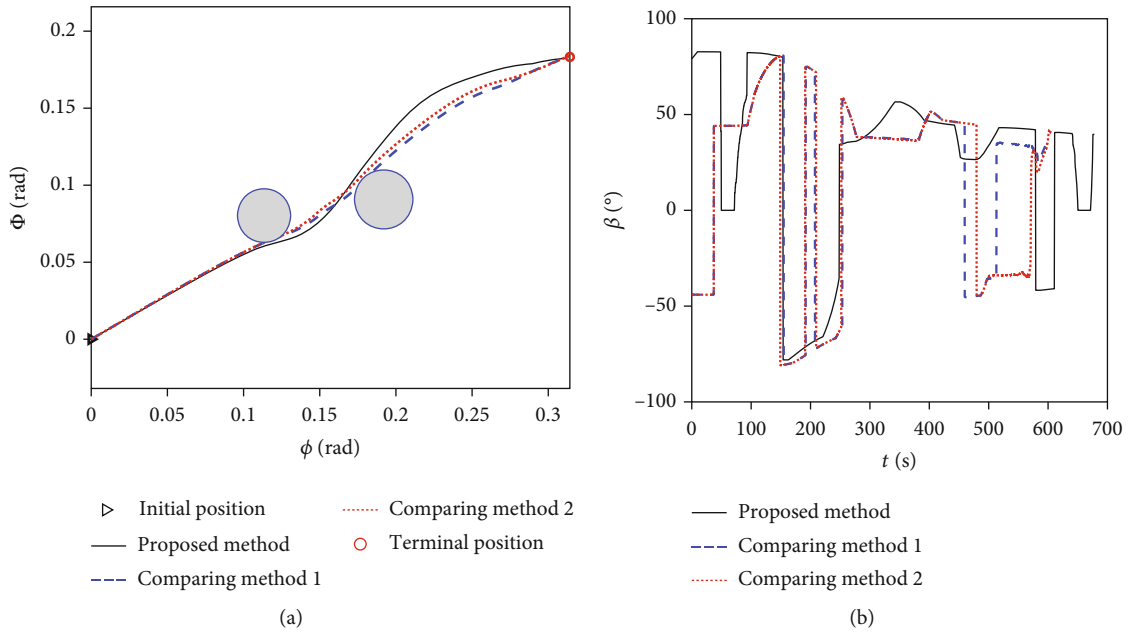


Figure 13: Guidance result with different guidance logic. (a) is the lateral guidance results with different guidance logic. (b) is the variation of bank angle with different guidance logic.

Table 5: Guidance results of different guidance methods.

| Method | $\Delta\phi_f(^\circ)$ | $\Delta\varphi_f(^\circ)$ | $\Delta h_f(km)$ | $E$ (km) | $F$ | $T$(s) |
|---|---|---|---|---|---|---|
| Proposed method | $7.7e-4$ | -0.006 | -1.724 | 1.830 | 5 | 7.74 |
| Comparing method 1 | -0.004 | 0.013 | -0.974 | 1.940 | 8 | 48.33 |
| Comparing method 2 | -0.019 | -0.036 | -0.418 | 4.507 | 8 | 48.83 |

sign changing of bank angle. It can be seen from Figure 9(a) that the crossrange corridor is symmetrical and the boundary changes slowly. It can be seen from Figures 8, 9(b), 9(c) that, despite the existence of no-fly zones, the amount of sign change of bank angle does not increase through adaptive crossrange corridor logic, and crossrange is always within the adaptive crossrange corridor. The crossrange corridor boundaries and crossrange realize convergence eventually, which verifies the validity of the proposed method. In conclusion, through the adaptive crossrange corridor in this paper, the crossrange of vehicle is always located inside the corridor, which can effectively ensure the lateral guidance.

The simulation results are shown as Table 2. Where $E$ represents guidance error of vehicle, the calculation equation is $E = \sqrt{((\Delta\phi_f)^2 + (\Delta\varphi_f)^2)R_e^2 + \Delta h_f^2}$. $\Delta\phi_f, \Delta\varphi_f, \Delta h_f$ represent the guidance error of longitude, latitude, and height, respectively. It can be seen from Table 2, whether there is no-fly zones, the guidance error is less than 5 km when the lateral and longitudinal guidance are always can be realized.

*5.2.3. Simulation with Different Initial Position.* In order to verify the guidance effect of proposed method in this paper further. The guidance result with different initial positions of vehicle are simulated under the same no-fly zone conditions and terminal positions, in which the no-fly zone is setting as same as case 2 in (1). The simulation condition and results are shown in Figure 10 and Table 3. The number of bank angle's sign changing is defined in Table 3 as $F$.

It can be seen from Figures 10(a) and 10(b) that vehicle can realize guidance with different initial positions, and the flight trajectories have different variation law. On the other hand, when the trajectory was affected slightly by the no-fly zone, vehicle's trajectory is closer to the no-fly zone according to crossrange corridor. And as vehicle flied closer to the no-fly zone, the crossrange reached the boundary of corridor rapidly and the sign of bank angle changed to avoid the no-fly zone. And from Figure 10(c), it was found that all the crossrange of trajectories can converge to 0 eventually by the adaptive crossrange corridor. And analyzing the guidance error with different initial position from Table 3, all the trajectories guidance error is less than 5 km when the longitudinal guidance error is less than 2 km. What is more, the change number of bank angle's sign is even less when vehicle need to avoid the no-fly zone with the adaptive crossrange corridor.

*5.2.4. Simulation with the Different Initial State.* In order to verify the robustness of the guidance method in this paper further, the simulation are operated when the initial state of the vehicle is disturbed. The simulation include the initial

height $\Delta h_0 = -2$km, initial speed $\Delta v_0 = +100m/s$, initial flight path angle $\Delta\theta_0 = +0.5^o$, and initial heading angle $\Delta\psi_0 = -10^o$. By this simulation, the initial state's influence on guidance results can be analyzed. The simulation results are shown in Figure 11, when guidance errors with different initial state are shown in Table 4.

Simulation results show that vehicle can still realize guidance and avoidance of no-fly zones with the disturbed initial state. As the initial flight path angle and velocity increase, the energy of the vehicle increases and the flight range increases. And when the height decreases, vehicle is also can be effectively guided as the flight range decreasing; on the other hand, even though trajectory of the vehicle changes greatly when the initial heading angle changes, it can still avoid the no-fly zones effectively. It can be seen from Table 3 that changing the heading angle has a greater impact on the guidance accuracy, which is reflected in the decrease of lateral guidance accuracy.

*5.2.5. Simulation with Disturbed Reentry Process.* Consider the guidance result of our method with disturbed reentry process. In this paper, 150 Monte Carlo simulations are carried out where no-fly zones are set as same as case 3 in (1) under the 20% uniform distribution of atmospheric deviation, 5% uniform distribution of deviation mass and stressed area, and 5% uniform distribution of lift and drag coefficient deviation. The results are shown in Figure 12. Most of the results show that the longitudinal guidance error is less than 2 km, and the most of lateral guidance error are within 5 km when the maximum is less than 7 km. It shows that our guidance method is robust to reentry disturbance.

*5.2.6. Comparison of Guidance Methods.* To reflect adaptive crossrange and flight neural network's effects, compare proposed method with conventional predictor-corrector guidance method which realize longitudinal guidance by integral-iteration method, and realize the lateral guidance through crossrange corridor and heading deviation angle corridor when avoid no-fly zone refer to literature [26], which is named comparing method 1 and comparing method 2 in Figure 13 and Table 5. And the setting of simulation is as same as case 3 in (1). The guidance result is shown in Figure 13.

As can be seen from Figure 13, because the separation between lateral guidance logic and no-fly zone avoid logic for the traditional predictor-corrector guidance, the variation number of bank angle' sign is usually more than that of adaptive crossrange corridor; on the other hand, it also easy to result in failure to avoid the no-fly zones as shown in Figure 13. By using the adaptive crossrange algorithm in this paper, the vehicle can realize avoidance effectively when the lateral guidance is realized as well. The adaptive corridor is always keep a certain width to reduce the variation number of bank angle's sign. The guidance results of the three methods are shown in Table 5.

As can be seen from Table 5, with different guidance methods, vehicle can reach the terminal position finally. But the guidance accuracy of the proposed method is better than other methods. The separation of the two logic causes increasing of change number of bank angle's sign, which is meaning that the guidance logic is affected by the avoidance logic. The time of the algorithm combined with the flight range prediction network is only 7.74 s, whose speed improves greatly compared with the conventional longitudinal guidance method.

## 6. Conclusion

In this paper, according to long calculation time of the predicted flight range in traditional predictor-corrector method, the variation characteristic of the predicted flight range is analyzed firstly. Then, based on the structure of ResNet and the dynamic model, the flight range prediction block and flight range prediction network are designed to realize the fast longitudinal guidance; on the other hand, to solve the separation of the lateral guidance logic and the avoidance logic of no-fly zone, the concept of the no-fly zone crossrange and no-fly zone mapping crossrange are proposed; and the adaptive cross corridor is established according to the repulsion's definition in artificial potential field method and its convergence is analyzed. Finally, the simulation results show that the proposed guidance method can realize effective guidance in different no-fly zone situations and has robustness to the disturbed initial position, state, and the reentry process. Compared with other guidance logics, the proposed guidance method has less sign variation number of bank angle and faster running speed.

## Data Availability

The data sources from the references are all marked in this paper. And the parameters designed are all described in this paper. Therefore, the data in this paper has been fully covered and can be obtained.

## Conflicts of Interest

The authors declare that they have no conflicts of interest.

## Acknowledgments

This study was supported by the National Natural Science Foundation of China (Grant no. 62173339 and no. 61873278). And the mentioned received funding did not lead to any conflict of interests. The authors would like to thank the Air and Missile Defense College of Air Force Engineering University of China for helpful discussions on topics related to this work.

## References

[1] Y. Xie, L. Liu, G. Tang, and W. Zheng, "A reentry trajectory planning approach satisfying waypoint and no-fly zone constraints," in *Proceedings of 5th international conference on recent advances in space technologies-RAST2011*, pp. 241–246, Istanbul, Turkey, 2011.

[2] C. Luo, H. Lei, J. Li, and C. Zhou, "A new adaptive neural control scheme for hypersonic vehicle with actuators multiple constraints," *Nonlinear Dynamics*, vol. 100, no. 4, pp. 3529–3553, 2020.

[3] J. T. Zhang, X. L. Shao, W. D. Zhang, and J. Na, "Path-following control capable of reinforcing transient performances for

networked mobile robots over a single curve," *IEEE Transactions on Instrumentation and Measurement*, p. 1, 2022.

[4] X. L. Shao, J. T. Zhang, and W. D. Zhang, "Distributed Cooperative Surrounding Control for Mobile Robots With Uncertainties and Aperiodic Sampling," *IEEE Transactions on Intelligent Transportation Systems*, vol. 23, no. 10, pp. 18951–18961, 2022.

[5] W. H. Zhang, X. L. Shao, W. D. Zhang, J. Qi, and H. Li, "Unknown input observer-based appointed-time funnel control for quadrotors," *Aerospace Science and Technology*, vol. 126, no. 107351, p. 107351, 2022.

[6] Z. Wang and M. J. Grant, "Constrained trajectory optimization for planetary entry via sequential convex programming," *Journal of Guidance Control & Dynamics*, vol. 40, no. 10, pp. 2603–2615, 2017.

[7] X. Zhou, H. B. Zhang, R. Z. He, G. J. Tang, and W. M. Bao, "Entrytrajectory planning method based on 3D profile via convex optimization," *Acta Aeronautica et Astronautica Sinica*, vol. 41, no. 11, pp. 66–82, 2020.

[8] X. Zhou, R. Z. He, H. B. Zhang, G. J. Tang, and W. M. Bao, "Sequential convex programming method using adaptive mesh refinement for entry trajectory planning problem," *Aerospace Science and Technology*, vol. 109, article 106374, 2020.

[9] M. M. Ali and P. Haijun, "A robust pseudospectral method for numerical solution of nonlinear optimal control problems," *International Journal of Computer Mathematics*, vol. 98, no. 6, pp. 1146–1165, 2021.

[10] N. Li, H. Lei, L. Shao, T. Liu, and B. Wang, "Trajectory optimization based on multi-interval mesh refinement method," *Mathematical Problems in Engineering*, vol. 2017, 8 pages, 2017.

[11] H. Y. Zhou, X. G. Wang, and N. G. Cui, "Glide trajectory optimization for hypersonic vehicles via dynamic pressure control," *Acta Astronautica*, vol. 164, pp. 376–386, 2019.

[12] L. Bryant, M. Tigges, and D. Ives, "Analytic drag control for precision landing and aerocapture," in *23rd Atmospheric Flight Mechanics Conference*, Boston,MA,U.S.A., 1998.

[13] P. Lunghi, M. Lavagna, and R. Armellin, "A semi-analytical guidance algorithm for autonomous landing," *Advances in Space Research*, vol. 55, no. 11, pp. 2719–2738, 2015.

[14] X. U. Mingliang, K. J. Chen, L. H. Liu, and G. Tang, "Quasi-equilibrium glide adaptive guidance for hypersonic vehicles," *Science China (Technological Sciences)*, vol. 55, no. 3, pp. 856–866, 2012.

[15] S. Xue and L. Ping, "Constrained predictor-corrector entry guidance," *Journal of Guidance Control and Dynamics*, vol. 33, no. 4, pp. 1273–1281, 2010.

[16] P. Lu, C. W. Brunner, S. J. Stachowiak, G. F. Mendeck, M. A. Tigges, and C. J. Cerimele, "Verification of a fully numerical entry guidance algorithm," *Journal of Guidance Control Dynamics*, vol. 39, no. 1, pp. 1–10, 2016.

[17] L. Ping, "Predictor-corrector entry guidance for low-lifting vehicles," *Journal of Guidance, Control, and Dynamics*, vol. 1, no. 4, pp. 1067–1075, 2008.

[18] W. Tao, H. Zhang, and G. Tang, "Predictor-corrector guidance for entry vehicle based on fuzzy logic," *Proceedings of the Institution of Mechanical Engineers Part G Journal of Aerospace Engineering*, vol. 233, no. 2, pp. 472–482, 2017.

[19] Z. Xiaofeng, Z. Huiping, Y. W. Hongylun, and S. Xingling, "Improved secant method-based predictive eentry guidance for hypersonic vehicle," *Tactical Missile Technology*, vol. 1, p. 8, 2016.

[20] L. Cheng, Z. Wang, Y. Cheng, Q. Zhang, and K. Ni, "Multi-constrained predictor-corrector reentry guidance for hypersonic vehicles," *Proceedings of the Institution of Mechanical Engineers, Part G: Journal of Aerospace Engineering*, vol. 232, no. 16, pp. 3049–3067, 2018.

[21] L. Zang, D. Lin, S. Chen, H. Wang, and Y. Ji, "An on-line guidance algorithm for high L/D hypersonic reentry vehicles," *Aerospace Science and Technology*, vol. 89, no. JUN., pp. 150–162, 2019.

[22] Z. Da, L. Lei, and Y. Wang, "On-line reentry guidance algorithm with both path and no-fly zone constraints - science direct," *Acta Astronautica*, vol. 117, pp. 243–253, 2015.

[23] Z. Jili, L. Kai, F. Yazhuo, and S. Zhiyong, "A piecewise predictor-corrector re-entry guidance algorithm with no-fly zone avoidance," *Journal of Astronautics*, vol. 42, no. 1, pp. 122–131, 2021.

[24] Z. Jili, L. Kai, F. Yazhuo, and S. Zhiyong, "Predictor-corrector switching reentry guidance method based on neural network range estimation model," *Tactical Missile Technology*, vol. 5, pp. 93–100+164, 2020.

[25] E. M. Yong, W. Q. Qian, and K. F. He, "An adaptive predictor–corrector reentry guidance based on self-definition waypoints," *Aerospace Science and Technology*, vol. 39, pp. 211–221, 2014.

[26] Q. Wang, M. Ran, and Y. Zhang, "Reentry guidance for hypersonic vehicle based on predictor-corrector method," *Journal of Beijing University of Aeronautics and Astronautics*, vol. 39, pp. 1563–1567, 2013.

[27] K. Zhang, G. X. Shi, and P. Wang, "Predictor-corrector reentry guidance with crossrange dynamic constraint," *Journal of Astronautics*, vol. 41, no. 4, p. 9, 2020.

[28] J. Zhu, L. Liu, G. Tang, and W. Bao, "Highly constrained optimal gliding guidance," *Proceedings of the Institution of Mechanical Engineers Part G Journal of Aerospace Engineering*, vol. 229, no. 12, pp. 2321–2335, 2015.

[29] H. Lin, Y. Du, E. Mooij, and W. Liu, "Improved predictor-corrector guidance with hybrid lateral logic for no-fly zone voidance," in *2019 International Conference on Control, Automation and Information Sciences (ICCAIS)*, Chengdu, China, 2019.

[30] K. He, X. Zhang, S. Ren, and J. Sun, "Deep residual learning for image recognition," in *IEEE Conference on Computer Vision and Pattern Recognition (CVPR)*, pp. 770–778, Las Vegas, USA, 2016.

[31] J. C. Harpold and C. A. Graves Jr., *Shuttle entry guidance*, American Astronautical Society, Houston, TX, 1978.

[32] T. H. Phillips, "A Common aero vehicle (CAV) model, description, and employment guide, [M.S. thesis]," *Schafer Corporation for AFRL and AFSPC*, 2003.